

The stellar mass distribution of the Milky Way’s bar: an analytic model

Mattia C. Sormani,¹★ Ortwin Gerhard,² Matthieu Portail,³ Eugene Vasiliev,⁴ Jonathan Clarke²

¹ *Universität Heidelberg, Zentrum für Astronomie, Institut für theoretische Astrophysik, Albert-Ueberle-Str. 2, 69120 Heidelberg, Germany*

² *Max-Planck-Institut für Extraterrestrische Physik, Gießenbachstraße 1, D-85748 Garching, Germany*

³ *CAPE Analytics, Gottfried-Keller-Straße 35, D-81245 München, Germany*

⁴ *Institute of Astronomy, University of Cambridge, Madingley Rd, Cambridge, CB3 0HA, UK*

Accepted XXX. Received YYY; in original form ZZZ

ABSTRACT

We present an analytic model of the stellar mass distribution of the Milky Way bar. The model is obtained by fitting a multi-component parametric density distribution to a made-to-measure N-body model of Portail et al., constructed to match a variety of density and kinematics observational data. The analytic model reproduces in detail the 3D density distribution of the N-body bar including the X-shape. The model and the gravitational potential it generates are available as part of the software package AGAMA for galactic dynamics, and can be readily used for orbit integrations, hydrodynamical simulations or other applications.

Key words: Galaxy: centre – Galaxy: bulge – Galaxy: structure – Galaxy: kinematics and dynamics – galaxies: bar

1 INTRODUCTION

At the beginning of the 1990s it became established that the Milky Way (MW) is a barred galaxy (Blitz & Spergel 1991; Binney et al. 1991; Weiland et al. 1994; Stanek et al. 1994). During the following three decades, our knowledge of the dynamical structure of the Galactic bar has vastly increased thanks to near-infrared photometric observations (Binney et al. 1997; Launhardt et al. 2002; Ness & Lang 2016), star counts (Stanek et al. 1997; Skrutskie et al. 2006; Saito et al. 2011; Cao et al. 2013; Wegg et al. 2015; Coleman et al. 2020), line-of-sight velocity (Kunder et al. 2012; Nidever et al. 2012; Ness et al. 2013; Zoccali et al. 2014; Bovy et al. 2019) and proper motion (Sanders et al. 2019a,b; Clarke et al. 2019) data, as well as stellar (Fux 1997; Shen et al. 2010; Molloy et al. 2015; Portail et al. 2017a,b) and gas dynamical (Fux 1999; Bissantz et al. 2003; Sormani et al. 2015; Li et al. 2016, 2022) modelling.

Having an easily-computable representation of the density distribution of the Galactic bar and its associated gravitational field is important for a number of applications, such as orbit integrations (Stolte et al. 2014; Habing 2016; Price-Whelan et al. 2016; Queiroz et al. 2020; Wylie et al. 2021), hydrodynamical calculations of the response of the interstellar gas to a bar potential (Armillotta et al. 2019; Tress et al. 2020; Sormani et al. 2020), and the study of the effect of the bar resonances (Dehnen 2000; Monari et al. 2019; Binney 2020; Chiba et al. 2021). However, there is a lack of a synthetic model that summarises in a concise way our current knowledge of the mass distribution of the Milky Way bar resulting from the huge body of work mentioned above.

Portail et al. (2017a) (hereafter P17) constructed dynamical models of the Milky Way bar by integrating an N-body system and slowly adjusting the masses of the particles until the time-averaged density field and other model observables converged to prescribed data, us-

ing a made-to-measure (M2M) method (Syer & Tremaine 1996; de Lorenzi et al. 2007). The P17 models are constrained to reproduce a variety of stellar density and kinematic data, and they build upon previous reconstructions of the 3D bar density from red clump giant star counts (Wegg & Gerhard 2013; Wegg et al. 2015). P17’s overall best-fitting model had a pattern speed of $\Omega_p = 40 \text{ km s}^{-1} \text{ kpc}^{-1}$. The pattern speed is one of the most important parameters of the bar since it sets the location of the resonances. More recently, there has been evidence for somewhat lower values of Ω_p (Clarke et al. 2019; Binney 2020; Chiba & Schönrich 2021; Clarke & Gerhard 2021). Here we consider the P17 model with $\Omega_p = 37.5 \text{ km s}^{-1} \text{ kpc}^{-1}$ which is a good match to the VIRAC proper motions (Clarke et al. 2019) and, with gas dynamical modelling, to the observed distribution of cold gas in the (l, v) -diagram (Li et al. 2022). This model can therefore be considered a state-of-the-art model that takes into account most of the available constraints on the structure of the MW bar.

In this short research note we present a detailed 3D analytic fit to the stellar mass distribution of the dynamical model of P17. The analytic model can reproduce the 3D N-body density accurately, including the X-shape. The analytic model and its associated gravitational potential are available as part of the software package AGAMA for galactic dynamics (Vasiliev 2019).

2 THE MODEL

The analytic model is composed by four components: three barred components, and an axisymmetric disc. The total density is:

$$\rho(x, y, z) = \underbrace{\rho_{\text{bar},1}}_{\text{bar}} + \underbrace{\rho_{\text{bar},2} + \rho_{\text{bar},3}}_{\text{long bar}} + \rho_{\text{disc}}. \quad (1)$$

The first two components together represent the bulge/bar (hereafter simply “bar”), i.e. the X-shaped boxy component in the centre. The third component represents the long bar, i.e. a vertically flat extension

★ E-mail: mattia.sormani@uni-heidelberg.de

of the bar which contribute to the “ears”, or bright enhancements at the ends, also known as “ansae” in the literature of external galaxies (e.g. Buta 2013). Note however that this decomposition is to some degree arbitrary and so these components only approximately correspond to the components with the same name in P17 and Wegg et al. (2015) (see also Sect. 4).

The first term on the right-hand side of Equation (1) is a modification of equation 9 of Coleman et al. (2020), which in turn is a generalisation of equation 10 of Freudreich (1998):

$$\rho_{\text{bar},1}(x, y, z) = \rho_1 \operatorname{sech}(a^m) \left[1 + \alpha \left(e^{-a_+^n} + e^{-a_-^n} \right) \right] e^{-\left(\frac{r}{r_{\text{cut}}}\right)^2}, \quad (2)$$

where

$$a = \left\{ \left[\left(\frac{|x|}{x_1} \right)^{c_\perp} + \left(\frac{|y|}{y_1} \right)^{c_\perp} \right]^{\frac{c_\parallel}{c_\perp}} + \left(\frac{|z|}{z_1} \right)^{c_\parallel} \right\}^{\frac{1}{c_\parallel}}, \quad (3)$$

$$a_\pm = \left[\left(\frac{x \pm cz}{x_c} \right)^2 + \left(\frac{y}{y_c} \right)^2 \right]^{\frac{1}{2}}, \quad (4)$$

$$r = (x^2 + y^2 + z^2)^{\frac{1}{2}}. \quad (5)$$

The parameter α quantifies the strength of the X-shape, while the parameter c quantifies its slope in the (x, z) plane.

The second and third terms on the right-hand side of Equation (1) have the same functional form, which is a modification of equation 9 of Wegg et al. (2015):

$$\rho_{\text{bar},i}(x, y, z) = \rho_i e^{-a_i^{n_i}} \operatorname{sech}^2\left(\frac{z}{z_i}\right) e^{-\left(\frac{R}{R_{i,\text{out}}}\right)^{n_{i,\text{out}}}} e^{-\left(\frac{R_{i,\text{in}}}{R}\right)^{n_{i,\text{in}}}}, \quad (6)$$

where $i = \{2, 3\}$ and

$$a_i = \left[\left(\frac{|x|}{x_i} \right)^{c_{\perp,i}} + \left(\frac{|y|}{y_i} \right)^{c_{\perp,i}} \right]^{\frac{1}{c_{\perp,i}}}, \quad (7)$$

$$R = (x^2 + y^2)^{\frac{1}{2}}. \quad (8)$$

The disc is an axisymmetric component that covers the region outside the bar. We take its density distribution to be:

$$\rho_{\text{disc}}(R, z) = \frac{\Sigma_0}{4z_d} e^{-\left(\frac{R}{R_d}\right)^{n_d}} e^{-\frac{R_{\text{cut}}}{R}} \operatorname{sech}\left(\frac{|z|}{z_d}\right)^{m_d}. \quad (9)$$

where R is the cylindrical radius given by Equation (8).

We fit the multi-component density distribution given by (1) to the time-averaged stellar density of the P17 M2M N-body model. The model of P17 originally has 10^6 stellar particles; its time-averaged density was computed on the fly during the fitting run on a 3D grid with spacing $\Delta x = \Delta y = 0.3$ kpc and $\Delta z = 0.1$ kpc. In this way the effective particle number is increased $\sim 100\times$, allowing for a much smoother density distribution. We then minimise the quantity $\Delta^2 = \sum_i (\rho_{\text{analytic},i} - \rho_{\text{N-body},i})^2$ using a standard Nelder-Mead algorithm, where $\rho_{\text{analytic},i}$ is the density of the analytic model, $\rho_{\text{N-body},i}$ is the time-averaged density of the P17 N-body model, and the sum is extended over all points i of the 3D grid.

3 RESULTS

The best-fitting parameters are reported in Table 1. The statistical uncertainties on the parameters are negligibly small and not very meaningful, since those stemming from the chosen functional form

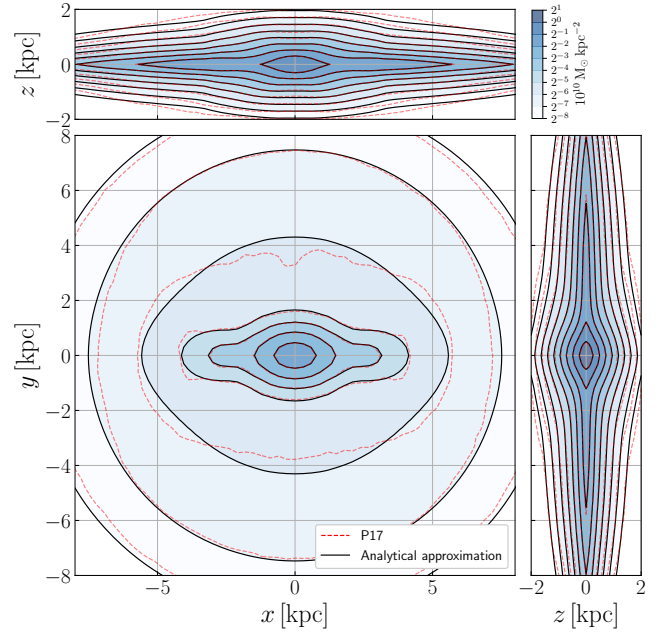


Figure 1. Surface density of the best-fitting analytic model compared to the time-averaged 3D density of the N-body model of P17.

parameter	value	units	parameter	value	units
Barred component 1			Disc		
ρ_1	0.316	$10^{10} M_\odot \text{ kpc}^{-3}$	Σ_0	0.103	$10^{10} M_\odot \text{ kpc}^{-2}$
x_1	0.490	kpc	R_d	4.754	kpc
y_1	0.392	kpc	z_d	0.151	kpc
z_1	0.229	kpc	R_{cut}	4.688	kpc
c_\parallel	1.991		n_d	1.536	
c_\perp	2.232		m_d	0.716	
m	0.873				
α	0.626				
n	1.940				
c	1.342				
x_c	0.751	kpc			
y_c	0.469	kpc			
r_{cut}	4.370	kpc			
Barred component 2			Barred component 3		
ρ_2	0.050	$10^{10} M_\odot \text{ kpc}^{-3}$	ρ_3	1743.049	$10^{10} M_\odot \text{ kpc}^{-3}$
x_2	5.364	kpc	x_3	0.478	kpc
y_2	0.959	kpc	y_3	0.267	kpc
z_2	0.611	kpc	z_3	0.252	kpc
n_2	3.051		n_3	0.980	
$c_{\perp,2}$	0.970		$c_{\perp,3}$	1.879	
$R_{2,\text{out}}$	3.190	kpc	$R_{3,\text{out}}$	2.204	kpc
$R_{2,\text{in}}$	0.558	kpc	$R_{3,\text{in}}$	7.607	kpc
$n_{2,\text{out}}$	16.731		$n_{3,\text{out}}$	-27.291	
$n_{2,\text{in}}$	3.196		$n_{3,\text{in}}$	1.630	

Table 1. Parameters of the best-fitting analytic model.

of the density profiles are likely much larger. The total masses of the three barred components and of the disc are $M_{\text{bar},1} = 1.28 \times 10^{10} M_\odot$, $M_{\text{bar},2} = 0.33 \times 10^{10} M_\odot$, $M_{\text{bar},3} = 0.22 \times 10^{10} M_\odot$ and $M_{\text{disc}} = 3.19 \times 10^{10} M_\odot$ respectively. Figure 1 shows that the surface density of the analytic model provides an excellent fit to the surface density of the P17 N-body model. Figures 2 and 3 shows that the analytic fit reproduces in detail the 3D structure of the N-body model, includ-

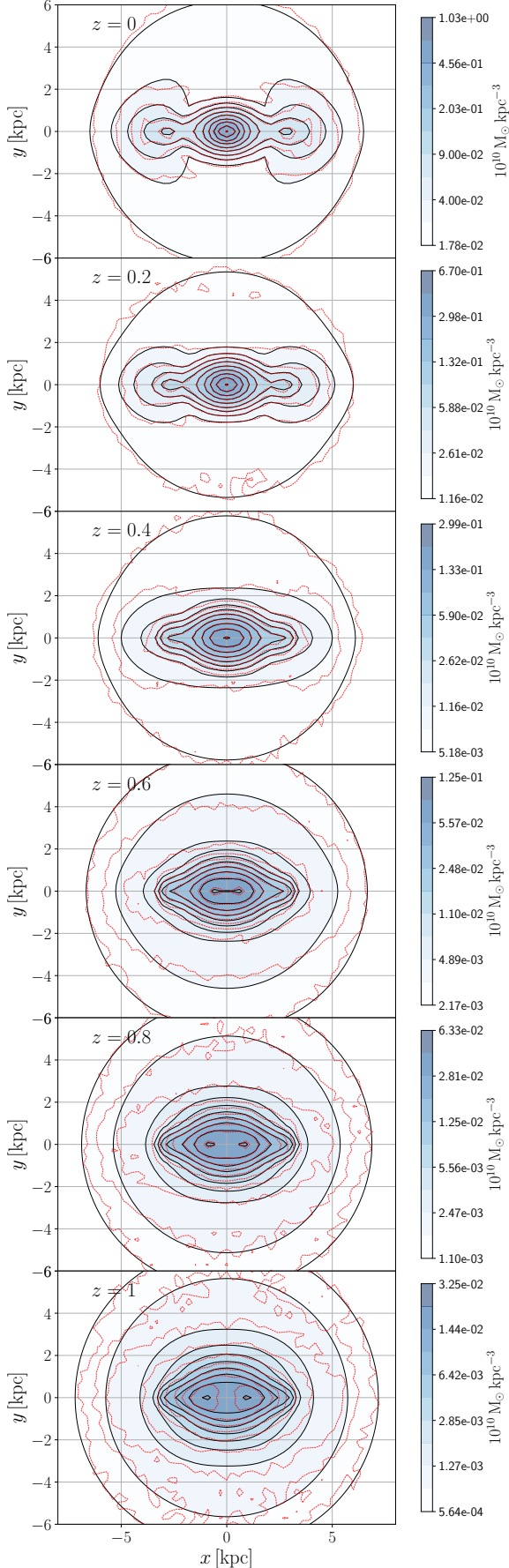


Figure 2. (x, y) density slices at fixed values of z of the analytic model (full black lines) compared to the P17 model (dashed red lines).

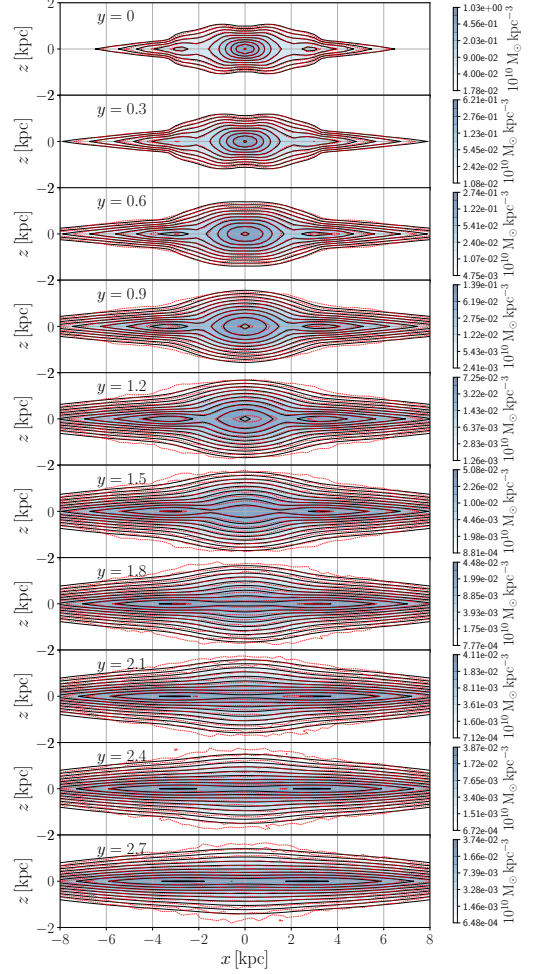


Figure 3. (x, z) density slices at fixed values of y of the analytic model (full black lines) compared to the P17 model (dashed red lines).

ing the X-shape. Figure 4 shows that the gravitational accelerations calculated with the analytic model reproduce well those of the P17 model, with an accuracy of the order of a few percent. The top panel shows the circular velocity curve, which quantifies the axisymmetric component of the bar and disc. The largest error ($\sim 5\%$) is observed at $R \sim 200$ pc, where the potential is actually dominated by the nuclear stellar disc. The latter is not included in the present model and should be added to obtain the total gravitational field at $R \lesssim 300$ pc (Sormani et al. 2022). Note also that this circular velocity curve does not include the dark matter component. The bottom panel shows the first 8 multipoles, which quantify the non-axisymmetric part of the potential. These are also approximated well by the analytical model. We have also checked that the potential is very well approximated also outside the plane $z = 0$. Finally, Fig. 5 compares the surface density along the x , y and z axes, while Fig. 6 dissects the surface density of the analytical model into its separate components.

4 DISCUSSION AND CONCLUSION

We have presented an analytic model of the stellar mass distribution of the Milky Way bar, obtained by fitting a made-to-measure N-body model of P17. The analytic model reproduces the 3D density distribution of the N-body model in detail, including the X-shape.

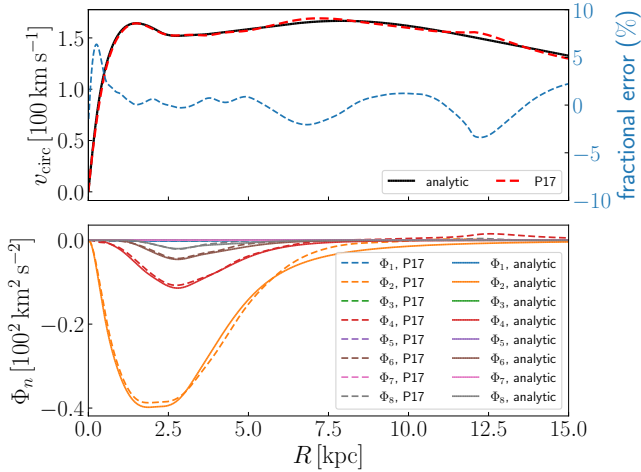


Figure 4. *Top:* Circular velocity curve of the analytical model compared to P17. The blue dashed line shows the fractional error $(v_{\text{circ,analytic}} - v_{\text{circ,P17}})/v_{\text{circ,P17}}$, which is of the order of few percent. *Bottom:* multipoles of the potential in the $z = 0$ plane, defined by expanding the potential as $\Phi(R, \theta) = \Phi_0(R) + \Phi_1(R) \cos(\theta) + \Phi_2(R) \cos(2\theta) + \dots$, where (R, θ) are planar Polar coordinates. The circular velocity is defined as $v_{\text{circ}} = \sqrt{Rd\Phi_0(R)/dR}$.

The model and the gravitational potential it generates are available as part of the software package Agama for galactic dynamics, and can be used for a number of applications, such as orbit integrations or hydrodynamical calculations of the response of the interstellar gas to a bar potential.

The distinction between “bar” and “long bar” in our fitting does not have an immediate physical meaning (e.g. in the sense that the two components correspond to two distinct orbital families, (Skokos et al. 2002; Harsoula & Kalapotharakos 2009; Wylie et al. 2021), and it should be merely seen as a convenient way of parametrising the density distribution. The bar + long bar components together can be considered as a meaningful component.

The P17 model was mainly fitted to data of the inner Galaxy and not to data of the outer disc. As such, the axisymmetric disc component might not represent the disc of the MW as accurately as other models available (e.g. McMillan 2017). Indeed, the disc of the P17 model produces a circular velocity that is slightly too low at the solar radius (Li et al. 2022). In some applications where a model of the gravitational potential of the Milky Way is needed, it might be convenient to replace the axisymmetric disc with a different model while keeping the bar + long bar components as presented here.

ACKNOWLEDGEMENTS

MSC acknowledges support from the Deutsche Forschungsgemeinschaft (DFG) via the Collaborative Research Center (SFB 881, Project-ID 138713538) “The Milky Way System” (sub-projects A1, B1, B2 and B8) and from the European Research Council in the ERC Synergy Grant “ECOGAL - Understanding our Galactic ecosystem: From the disk of the Milky Way to the formation sites of stars and planets” (project ID 855130).

DATA AVAILABILITY

The analytic fit and the associated gravitational potential are publicly available through the software package AGAMA (<https://github.com/GalacticDynamics-Oxford/Agama>).

REFERENCES

- Armillotta L., Krumholz M. R., Di Teodoro E. M., McClure-Griffiths N. M., 2019, *MNRAS*, **490**, 4401
- Binney J., 2020, *MNRAS*, **495**, 895
- Binney J., Gerhard O. E., Stark A. A., Bally J., Uchida K. I., 1991, *MNRAS*, **252**, 210
- Binney J., Gerhard O., Spergel D., 1997, *MNRAS*, **288**, 365
- Bissantz N., Englmaier P., Gerhard O., 2003, *MNRAS*, **340**, 949
- Blitz L., Spergel D. N., 1991, *ApJ*, **379**, 631
- Bovy J., Leung H. W., Hunt J. A. S., Mackereth J. T., García-Hernández D. A., Roman-Lopes A., 2019, *MNRAS*, **490**, 4740
- Buta R. J., 2013, *Galaxy Morphology*, p. 1, doi:10.1007/978-94-007-5609-0_1
- Cao L., Mao S., Nataf D., Rattenbury N. J., Gould A., 2013, *MNRAS*, **434**, 595
- Chiba R., Schönrich R., 2021, *MNRAS*, **505**, 2412
- Chiba R., Friske J. K. S., Schönrich R., 2021, *MNRAS*, **500**, 4710
- Clarke J., Gerhard O., 2021, arXiv e-prints, p. arXiv:2107.10875
- Clarke J. P., Wegg C., Gerhard O., Smith L. C., Lucas P. W., Wylie S. M., 2019, *MNRAS*, **489**, 3519
- Coleman B., Paterson D., Gordon C., Macias O., Ploeg H., 2020, *MNRAS*, **495**, 3350
- Dehnen W., 2000, *AJ*, **119**, 800
- Freudenreich H. T., 1998, *ApJ*, **492**, 495
- Fux R., 1997, *A&A*, **327**, 983
- Fux R., 1999, *A&A*, **345**, 787
- Habing H. J., 2016, *A&A*, **587**, A140
- Harsoula M., Kalapotharakos C., 2009, *MNRAS*, **394**, 1605
- Kunder A., et al., 2012, *AJ*, **143**, 57
- Launhardt R., Zylka R., Mezger P. G., 2002, *A&A*, **384**, 112
- Li Z., Gerhard O., Shen J., Portail M., Wegg C., 2016, *ApJ*, **824**, 13
- Li Z., Shen J., Gerhard O., Clarke J. P., 2022, *ApJ*, **925**, 71
- McMillan P. J., 2017, *MNRAS*, **465**, 76
- Molloy M., Smith M. C., Evans N. W., Shen J., 2015, *ApJ*, **812**, 146
- Monari G., Famaey B., Siebert A., Wegg C., Gerhard O., 2019, *A&A*, **626**, A41
- Ness M., Lang D., 2016, *AJ*, **152**, 14
- Ness M., et al., 2013, *MNRAS*, **432**, 2092
- Nidever D. L., et al., 2012, *ApJ*, **755**, L25
- Portail M., Gerhard O., Wegg C., Ness M., 2017a, *MNRAS*, **465**, 1621
- Portail M., Wegg C., Gerhard O., Ness M., 2017b, *MNRAS*, **470**, 1233
- Price-Whelan A. M., Sesar B., Johnston K. V., Rix H.-W., 2016, *ApJ*, **824**, 104
- Queiroz A. B. A., et al., 2020, arXiv e-prints, p. arXiv:2007.12915
- Saito R. K., Zoccali M., McWilliam A., Minniti D., Gonzalez O. A., Hill V., 2011, *AJ*, **142**, 76
- Sanders J. L., Smith L., Evans N. W., Lucas P., 2019a, *MNRAS*, **487**, 5188
- Sanders J. L., Smith L., Evans N. W., 2019b, *MNRAS*, **488**, 4552
- Shen J., Rich R. M., Kormendy J., Howard C. D., De Propris R., Kunder A., 2010, *ApJ*, **720**, L72
- Skokos C., Patsis P. A., Athanassoula E., 2002, *MNRAS*, **333**, 847
- Skrutskie M. F., Cutri R. M., Stiening R., Weinberg M. D., et al. 2006, *AJ*, **131**, 1163
- Sormani M. C., Binney J., Magorrian J., 2015, *MNRAS*, **454**, 1818
- Sormani M. C., Tress R. G., Glover S. C. O., Klessen R. S., Battersby C. D., Clark P. C., Hatchfield H. P., Smith R. J., 2020, *MNRAS*, **497**, 5024
- Sormani M. C., et al., 2022, *MNRAS*, **512**, 1857
- Stanek K. Z., Mateo M., Udalski A., Szymanski M., Kaluzny J., Kubiak M., 1994, *ApJ*, **429**, L73

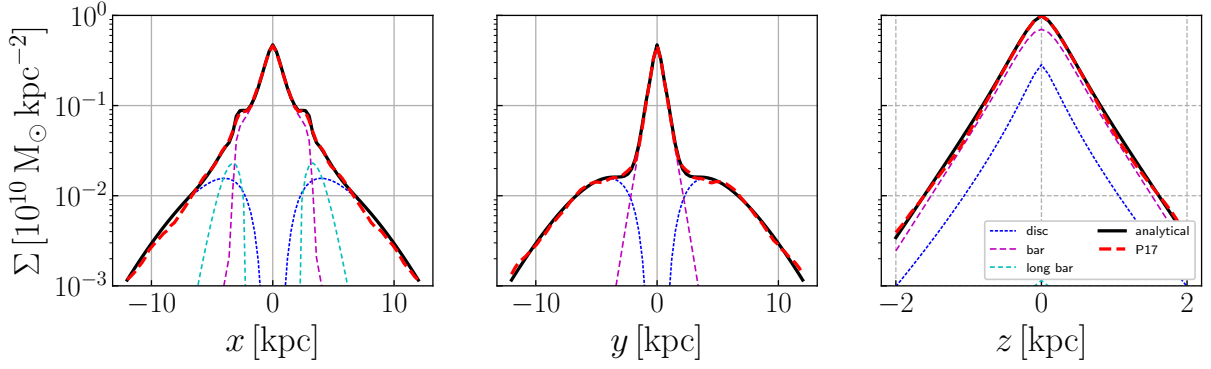


Figure 5. Surface density along the x , y or z axis of the analytic model (black full line) compared to the P17 made-to-measure N-body model (red dashed line). The left and middle panels correspond to the x and y axes in the (x, y) map in Fig. 1, while the right panel correspond to the z axis in the (x, z) map.

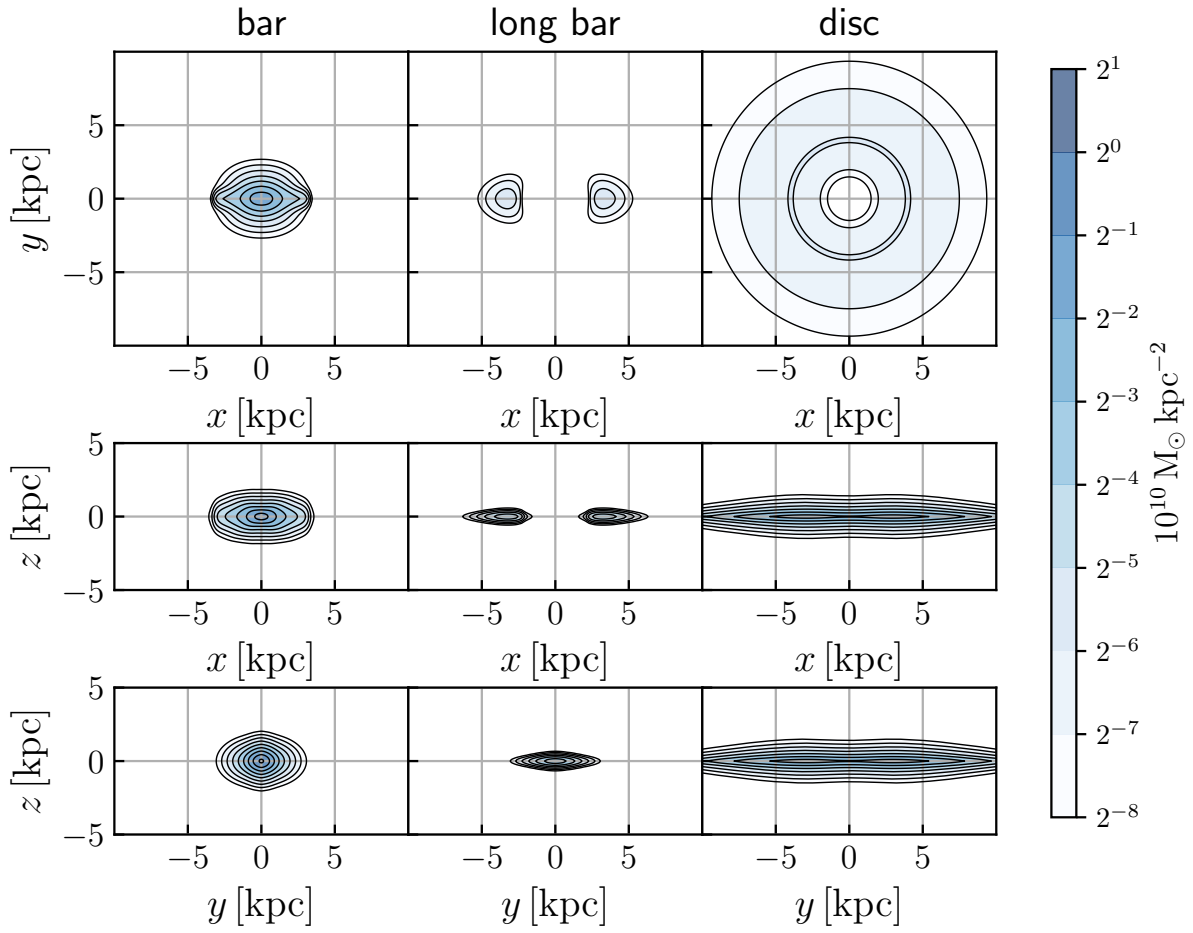


Figure 6. Surface density of the separate components of the analytical model.

Stanek K. Z., Udalski A., Szymański M., Kałużny J., Kubiak Z. M., Mateo M., Krzemiński W., 1997, *ApJ*, **477**, 163
 Stolte A., et al., 2014, *ApJ*, **789**, 115
 Syer D., Tremaine S., 1996, *MNRAS*, **282**, 223
 Tress R. G., Sormani M. C., Glover S. C. O., Klessen R. S., Battersby C. D., Clark P. C., Hatchfield H. P., Smith R. J., 2020, *MNRAS*, **499**, 4455
 Vasiliev E., 2019, *MNRAS*, **482**, 1525
 Wegg C., Gerhard O., 2013, *MNRAS*, **435**, 1874
 Wegg C., Gerhard O., Portail M., 2015, *MNRAS*, **450**, 4050

Weiland J. L., et al., 1994, *ApJ*, **425**, L81
 Wylie S. M., Clarke J. P., Gerhard O. E., 2021, arXiv e-prints, p. arXiv:2110.03658
 Zoccali M., et al., 2014, *A&A*, **562**, A66
 de Lorenzi F., Debattista V. P., Gerhard O., Sambhus N., 2007, *MNRAS*, **376**, 71

This paper has been typeset from a \LaTeX file prepared by the author.